

PNNL-34983 Rev 0 DVZ-RPT-102 Rev 0

Estimating Vadose Zone Flow Properties at the 100 K-East Soil Flushing Site Using ERT Monitoring Data: 2023 Interim Report

100 KE Soil Property Estimation September 2023

Tim Johnson Glenn Hammond Piyoosh Jaysaval Bryan He Rob Mackley



DISCLAIMER

This report was prepared as an account of work sponsored by an agency of the United States Government. Neither the United States Government nor any agency thereof, nor Battelle Memorial Institute, nor any of their employees, makes any warranty, express or implied, or assumes any legal liability or responsibility for the accuracy, completeness, or usefulness of any information, apparatus, product, or process disclosed, or represents that its use would not infringe privately owned rights. Reference herein to any specific commercial product, process, or service by trade name, trademark, manufacturer, or otherwise does not necessarily constitute or imply its endorsement, recommendation, or favoring by the United States Government or any agency thereof, or Battelle Memorial Institute. The views and opinions of authors expressed herein do not necessarily state or reflect those of the United States Government or any agency thereof.

PACIFIC NORTHWEST NATIONAL LABORATORY

operated by

BATTELLE

for the

UNITED STATES DEPARTMENT OF ENERGY

under Contract DE-AC05-76RL01830

Printed in the United States of America

Available to DOE and DOE contractors from the Office of Scientific and Technical Information, P.O. Box 62, Oak Ridge, TN 37831-0062

www.osti.gov ph: (865) 576-8401 fox: (865) 576-5728 email: reports@osti.gov

Available to the public from the National Technical Information Service 5301 Shawnee Rd., Alexandria, VA 22312 ph: (800) 553-NTIS (6847) or (703) 605-6000

email: info@ntis.gov
Online ordering: http://www.ntis.gov

Estimating Vadose Zone Flow Properties at the 100 K-East Soil Flushing Site Using ERT Monitoring Data: 2023 Interim Report

100 KE Soil Property Estimation

September 2023

Tim Johnson Glenn Hammond Piyoosh Jaysaval Bryan He Rob Mackley

Prepared for the U.S. Department of Energy under Contract DE-AC05-76RL01830

Pacific Northwest National Laboratory Richland, Washington 99354

Summary

In situ soil flushing is being using at the Hanford 100 K-East (100 KE) area to transport mobile chromium contamination in the vadose zone to the water table, where it can be collected and treat through pump and treat operations. The efficacy of soil flushing is directly related to the volume of clean water that infiltrates through contaminated soils. In practice, it is infeasible to comprehensively monitor which regions of the vadose zone are being infiltrated through direct sampling of pore water. Consequently, there can be significant uncertainty about which regions of the subsurface have been treated, especially if hydrogeologic conditions are favorable for the development of unstable flows and preferred flow pathways through the vadose zone (Jarvis, Koestel, and Larsbo 2016).

Current approaches for quantitative monitoring of soil flushing performance rely on contaminant concentration measurements collected from extractions wells. There is no quantitative information on the volume of flush water delivered to targeted regions of the vadose zone at the Hanford Site, leading to significant uncertainty regarding source term removal and long-term impacts to groundwater. If the subsurface hydrogeologic properties at the 100 KE Area were adequately known, qualitative metrics of soil flushing performance could be simulated, thereby negating expenses required to obtain quantitative performance information through borehole drilling/sampling. However, estimating in situ hydrogeologic properties has long proven elusive, due primarily to a lack of sufficient information to constrain heterogeneous property estimates to a useful degree of certainty. Estimating vadose zone hydrogeologic properties is particularly challenging due the dependence of hydraulic conductivity on saturation.

This report describes progress toward a first-of-its-kind demonstration using surface time-lapse 3D electrical resistivity tomography (ERT) monitoring data to estimate the hydrogeologic properties that control flush water transport at the 100 KE soil flushing site. The ultimate objective is (1) to verify sufficient information exists in the ERT monitoring data to adequately resolve vadose zone hydraulic properties, and (2) generate a "digital twin" (i.e., a numerical simulator) that can be used to simulate the amount of flush water that has been delivered to each targeted region of the vadose zone, and thereby assess the efficacy of flush water delivery. Resulting performance estimates can be used in leu of comprehensive borehole drilling and direct sampling (or wellbore logging) that would otherwise be required to obtain the same information.

Estimating the hydrogeologic properties that govern soil flushing behavior will ultimately be accomplished using new multi-physics joint inversion capabilities recently implemented in the high-performance parallel PFLOTRAN flow and reactive transport simulator. This report describes preparatory steps taken for the joint inversion, including development of a PFLOTRAN-trained deep neural network (DNN) designed to (1) assess the information content in the time-lapse ERT data in terms of resolving the governing hydrogeologic properties of the 100 KE soil flushing site, and (2) provide an accruing starting estimate of hydrogeologic parameters for the joint inversion.

Initial results of the DNN training and performance assessment suggest the time-lapse ERT data contains sufficient information to accurately estimate hydrogeologic properties if (1) hydrogeologic properties can be considered homogeneous within a given stratigraphic unit, (2) stratigraphic unit boundaries are well known, and (3) uniform application of flush water at the soil surface is an adequate approximate to actual flush water application. Given each of these assumptions, Figure S1 shows an example of the DNN-based prediction of soil saturation after 7 days of soil flushing, compared to the corresponding time-lapse ERT image of the change in bulk electrical conductivity, which represents the current state-of-the-art use of time-lapse ERT data. Both treatments show the influence of the interface between backfill and native formation soils, shown in the right image as a white line. Specifically, the interface acts as a vertical flow impediment, causing a redistribution of flush water to low points in the boundary.

Summary ii

In contrast to the imperfectly resolved ERT image, the DNN assessment is constrained by the physics of flow and transport and is therefore physically accurate. A version of the DNN-estimated hydrogeologic properties will serve as the starting estimate for the joint inversion, which will be conducted in 2024. The resulting digital twin will enable (through simulation) quantitative assessments of soil flushing behavior that are not currently possible, such as the transport pathways of flush water to the water table and the number of pore volumes of flush water treating a particular volume of soil. Finally, the calibrated digital twin will be used in a secondary inversion to constrain the possible location and contaminant concentrations of source zones within the treated volume.

We have thus far used multi-physics simulations and deep machine learning to demonstrate at a minimum that if (1) soil hydraulic properties can be considered homogenous within each of the three primary stratigraphic units in the system and (2) uniform application of flush water at the surface is a valid approximation, then there is sufficient information in the time-lapse ERT data to accurately estimate governing hydraulic properties of the backfill and Hanford formation, and to a lesser extent the Ringold Formation. An assessment of the uncertainty induced by assuming homogeneous stratigraphic units and uniform application of flush water will also be conducted in 2024.

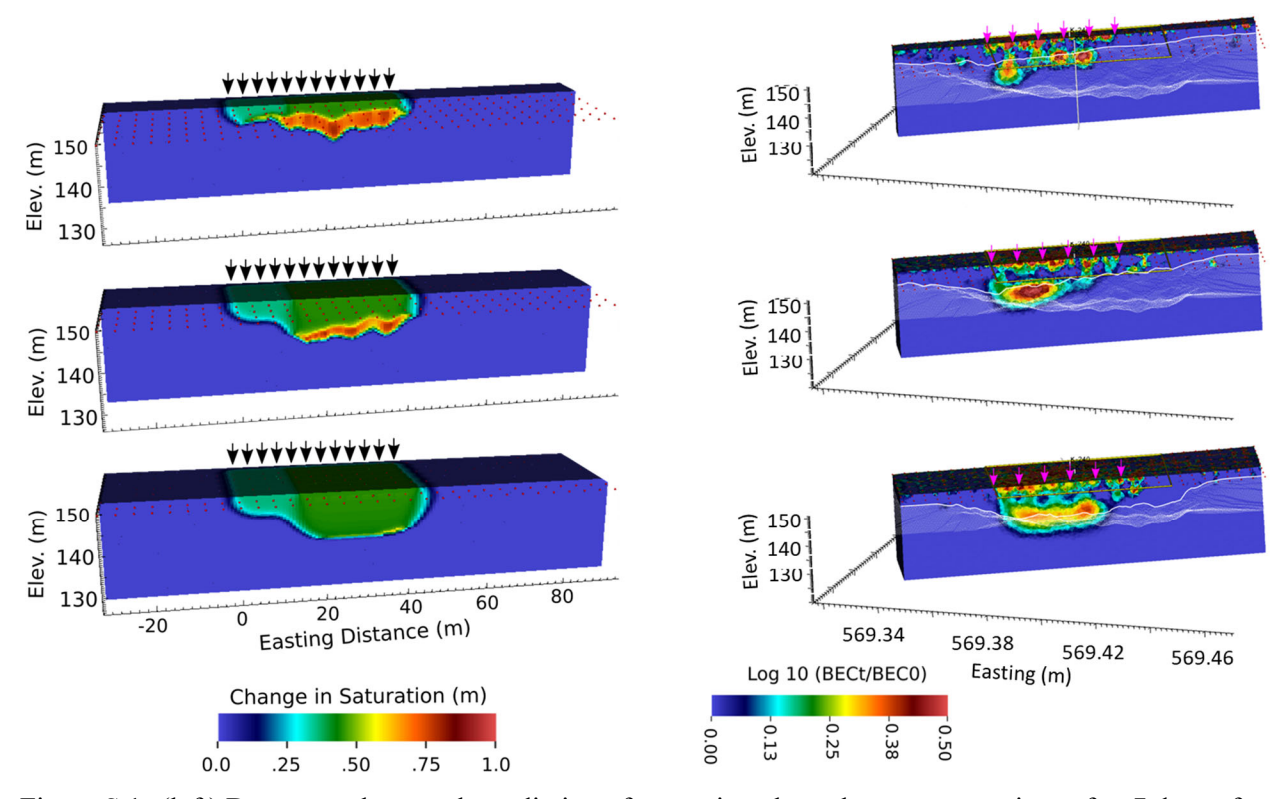


Figure S.1. (left) Deep neural network prediction of saturation along three cross-sections after 7 days of soil flushing compared to (right) time-lapse ERT images of changes in bulk electrical conductivity after 7 days of soil flushing.

Summary

Acknowledgments

This document was prepared by the Deep Vadose Zone – Applied Field Research Initiative at Pacific Northwest National Laboratory. Funding was provided by the U.S. Department of Energy (DOE) Richland Operations Office. Pacific Northwest National Laboratory is operated by Battelle Memorial Institute for the DOE under Contract DE-AC05-76RL01830.

Acknowledgments

Acronyms and Abbreviations

BEC bulk electrical conductivity

DNN deep neural network

ERT electrical resistivity tomography

PNNL Pacific Northwest National Laboratory

Contents

Summa	ary		ii			
Acknow	wledgme	ents	iv			
Acrony	ms and	Abbreviations	v			
1.0	Introdu	ction	1			
2.0	100 KE Soil Flushing Site and ERT Monitoring Array Summary					
3.0	Time-Lapse ERT Imaging Summary and Interpretation					
4.0	ERT-Based Deep Neural Network Training and Prediction of Field Soil Flushing Behavior					
5.0	Discussion and Next Steps					
6.0	References					
Figu	ıres					
Figure	1.	Historical images of the 100 KE Area showing unplanned releases from the sodium dichromate storage tank located in the K East contaminated vadose zone soils, which presently act as a slow-release source zone for groundwater chromium contamination.	3			
Figure	2.	(top) Aerial view of the excavation pit constructed to remove chromium-contaminated sediments from the vadose zone. (bottom) Aerial of the soil flushing zone superimposed on the backfilled excavation pit.	4			
Figure	3.	Location of surface ERT electrode lines (black dots) installed over the soil flushing zone. The lateral extent of the array, which impacts imaging depth of investigation, was limited by the building foundation located at the eastern margin of the array	5			
Figure	4.	(top) Oblique view of the boundary between the pit backfill and the Hanford formation. (bottom) Cross section showing the approximate position of the water table, the Ringold Formation, the Hanford-Ringold formation contact, and the contact between the Hanford formation and pit backfill	6			
Figure	5.	A) Flush water application zones and B) application rates over time in each zone within the infiltration gallery.	7			
Figure 6.		(left) Photograph taken during the first week of soil flushing, highlighting the distribution of flush water lines and shallow surface water ponding cause by slight variations in topography. (right) Photograph highlighting the ERT electrode array (white boxes connected by cables)				
Figure 7.		Summary of time-lapse ERT images after the first 7 days of flushing, highlighting the development of preferential flow paths within the pit backfill soils and redistribution of flush water along the pit boundary. Magenta arrows indicate the active flushing zone for the previous 7 days. White dappled surface is the pit boundary, and the white line denotes the pit boundary projected on the cross-section.				
Figure	8.	Summary of time-lapse ERT images after the first 14 days of flushing, highlighting the development of preferential flow paths within the pit backfill soils and redistribution of flush water along the pit boundary. Magenta arrows				

Contents

	indicate the active flushing zone for the previous 7 days. White dappled surface is the pit boundary, and the white line denotes the pit boundary projected on the cross-section	12
Figure 9.	Summary of time-lapse ERT images after the first 21 days of flushing, highlighting the development of preferential flow paths within the pit backfill soils and redistribution of flush water along the pit boundary. Magenta arrows indicate the active flushing zone for the previous 7 days. White dappled surface is the pit boundary, and the white line denotes the pit boundary projected on the cross-section.	13
Figure 10.	Summary of time-lapse ERT images after the first 28 days of flushing, highlighting the development of preferential flow paths within the pit backfill soils and redistribution of flush water along the pit boundary. Magenta arrows indicate the active flushing zone for the previous 7 days. White dappled surface is the pit boundary, and the white line denotes the pit boundary projected on the cross-section.	14
Figure 11.	Flow diagram showing training and application of a deep neural network for prediction of soil flushing behavior using field ERT monitoring data.	15
Figure 12.	(left) Cross-sections of DNN-predicted change in saturation from north (top) to south (bottom) after 7 days of flushing in west and center flushing zones. (right) Stratigraphic cross-section.	18
Figure 13.	(left) Cross-sections of DNN-predicted change in saturation from north (top) to south (bottom) after 14 days of flushing. Center and east flushing zones were active from day 7 to day 14 (see Figure 5). (right) Stratigraphic cross-sections corresponding to each saturation cross-section	19
Figure 14.	(left) Cross-sections of DNN-predicted change in saturation from north (top) to south (bottom) after 21 days of flushing. Center and west flushing zones were active from day 14 to day 21 (see Figure 5). (right) Stratigraphic cross-sections corresponding to each saturation cross-section	19
Figure 15.	(left) Cross-sections of DNN-predicted change in saturation from north (top) to south (bottom) after 28 days of flushing. All flushing zones were active from day 21 to day 28 (see Figure 5). (right) Stratigraphic cross-sections corresponding to each saturation cross-section.	20
Tables		
Table 1.	DNN-predicted 100 KE soil hydraulic properties and petrophysical parameters	17

Contents

1.0 Introduction

Former operations in the 100 KE Area at the Hanford Site resulted in hexavalent chromium in the vadose zone that provides a source of groundwater contamination. Contaminated groundwater is currently being hydraulically captured, removed, and transported to a pump-and-treat facility through a series of extraction wells. Although these current mitigation procedures are protective of the Columbia River, vadose zone soils within the 100 KE Area are expected to provide a continued source of groundwater chromium that may prevent site closure for decades.

Soil flushing is being used at the 100 KE Area to accelerate the removal of the chromium source zone. Soil flushing works by applying a continuous stream of clean water at the surface and allowing it to percolate to the water table. As the water migrates downward through contaminated soil, it transports the chromium from contaminated vadose zone soil to the groundwater, where it is removed through pump-and-treat extraction. The efficacy of soil flushing is directly related to the volume of clean water that infiltrates through contaminated soils. In practice, it is infeasible to comprehensively monitor which regions of the vadose zone are being infiltrated through direct sampling of pore water. Consequently, there can be significant uncertainty about which regions of the subsurface have been treated, especially if hydrogeologic conditions are favorable for the development of unstable flows and preferred flow pathways through the vadose zone (Jarvis, Koestel, and Larsbo 2016).

Time-lapse electrical resistivity tomography (ERT) imaging is a method of remotely imaging spatial and temporal changes in the bulk electrical conductivity (BEC) of the subsurface. Because BEC is governed in part by soil saturation, 3D time-lapse ERT can be an effective tool for monitoring when and where the vadose zone is impacted by flush water. ERT works by injecting electrical currents and measuring electrical potentials (i.e., voltages) on an array of electrodes installed (in this case) along the ground surface. ERT data is then numerically processed to produce an imperfectly resolved image of subsurface BEC. In monitoring applications, ERT data is collected on a repeating schedule and processed to produce images of changes in BEC over time. During soil flushing, increases in BEC with respect to background conditions are diagnostic of increased soil moisture. Time-lapse images of increases in BEC may therefore be interpreted to diagnose when and where flush water has reached a given region of the vadose zone.

Although time-lapse ERT monitoring can significantly enhance soil flushing performance monitoring compared to the use of boreholes alone, it only provides quantitative and limited-resolution information regarding the distribution of flush water at a given point in space and time. Time-lapse ERT cannot provide quantitative performance information, such as the total volume of flush water that has percolated through a given region of the subsurface at a given time. Ideally, soil flushing performance could be analyzed through accurate numerical simulation. However, as with most subsurface flow and transport simulations, there is insufficient data to adequately constrain estimates of the hydrogeological properties that govern vadose zone flow, and therefore to simulate flow with enough certainty to provide a useful approximation of flushing performance under heterogeneous field conditions.

Recognizing the significant but implicit information regarding governing hydrogeological properties embedded in time-lapse ERT data, Pacific Northwest National Laboratory (PNNL) recently dedicated Laboratory Directed Research and Development funding to develop numerical tools that enable ERT monitoring data to directly inform flow and transport simulations. In essence, a high-performance flow and transport simulator (PFLOTRAN) (Jaysaval, Hammond, and Johnson 2023) simulates the raw ERT data collected during flushing operations, and then systematically modifies governing hydrogeologic properties until the simulated ERT data honors both the observed ERT data and any other traditional sources of monitoring data (e.g., flush water application rates and locations, flush water fluid conductivity). The ultimate objective of the analysis is to generate a calibrated "digital twin" of the soil

Introduction 1

flushing system that honors all available characterization and monitoring data, and can be used to (among other things) quantitatively simulate flushing performance metrics (e.g., the number of pore volumes of flush water that passed through a given region of the subsurface).

In this interim report, we describe progress toward generating an accurate numerical model (i.e., the digital twin) that can be used to quantitively approximate soil flushing behavior at the 100 KE site by estimating the in situ unsaturated hydraulic properties that govern transport. The analysis first involves an assessment of the information content in the ERT data in terms of its capability to estimate unsaturated hydraulic parameters within the three primary stratigraphic units at the 100 KE site. Next, we use the ERT data to estimate the hydraulic properties that govern flush water flow and the petrophysical parameters that relate BEC to hydraulic properties and subsurface states (e.g., porosity, saturation, and pore fluid conductivity). When provided as input parameters into a PFLOTRAN simulation of soil flushing behavior, the simulation will accurately predict the ERT data, and presumably the flush water migration that controls the ERT response. Initial results suggest that flush water transport is influenced by the presence of pit backfill soils. Specifically, flush water is redirected along the interface between the higher permeability backfill sediments and the lower permeability Hanford formation. Continuing efforts are underway to refine the parameter estimates, develop estimates of uncertainty, and demonstrate how the 100 KE digital twin can be used to provide quantitative estimates of flushing.

Introduction 2

2.0 100 KE Soil Flushing Site and ERT Monitoring Array Summary

Figure 1 shows three historical images of the Hanford 100 KE Area. The 100 KE Area includes the K East Reactor and supporting facilities, including a sodium dichromate storage tank and transport piping in the annotated area in the Figure 1 photos from 1964 and 2017. Sodium dichromate was used to inhibit piping corrosion. During operations, releases of sodium dichromate occurred in the K East Area, contaminating vadose zone sediments and creating a slow-release source zone of chromium to the groundwater.

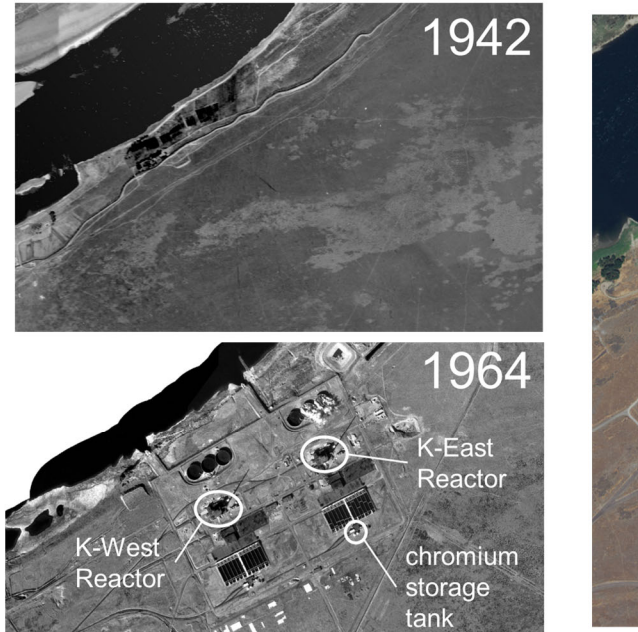




Figure 1. Historical images of the 100 KE Area showing unplanned releases from the sodium dichromate storage tank located in the K East contaminated vadose zone soils, which presently act as a slow-release source zone for groundwater chromium contamination.

Initial efforts to remediate chromium-contaminated vadose zone sediments involved excavating contaminated soils. Excavation proceeded by testing soils at the bottom of the excavation pit for chromium, and excavating where contaminated soils were located. Maintaining side-slopes required for geotechnical stability became infeasible after the pit reached a certain depth, and the pit was filled with clean backfill.

After the excavation pit was backfilled, soil flushing was chosen to remediate contaminated sediments remaining beneath the pit boundary. Figure 2 (top) shows an aerial image of the pit taken near the end of excavation operations. Figure 2 (bottom) shows the flush zone boundary superimposed on an aerial image of the post-backfill excavation zone. Clean flush water was sourced from the 200 West Area pump-and-treat system effluent and applied at the ground surface with an array of dispersion hoses distributed within the flush zone.

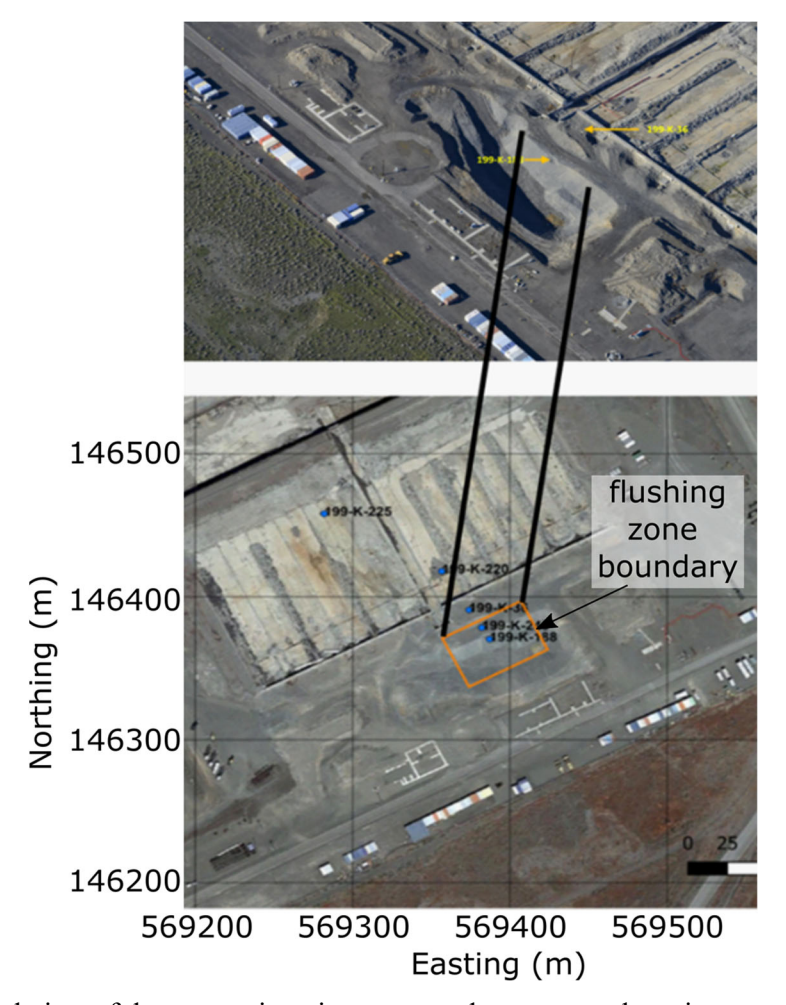


Figure 2. (top) Aerial view of the excavation pit constructed to remove chromium-contaminated sediments from the vadose zone. (bottom) Aerial of the soil flushing zone superimposed on the backfilled excavation pit.

To monitor the migration of flush water through the vadose zone, a surface-based ERT electrode array was installed over the flush zone as shown in Figure 3. The array consisted of 8 lines of 32 electrodes each, with 4-m spacing between electrodes and 5.4-m spacing between lines. ERT imaging depth is determined in large part by the length of the array. In this case, the line lengths were limited by the building foundation located on the eastern margin of the array. Consequently, imaging depth was limited to approximately 20 m below the ground surface.

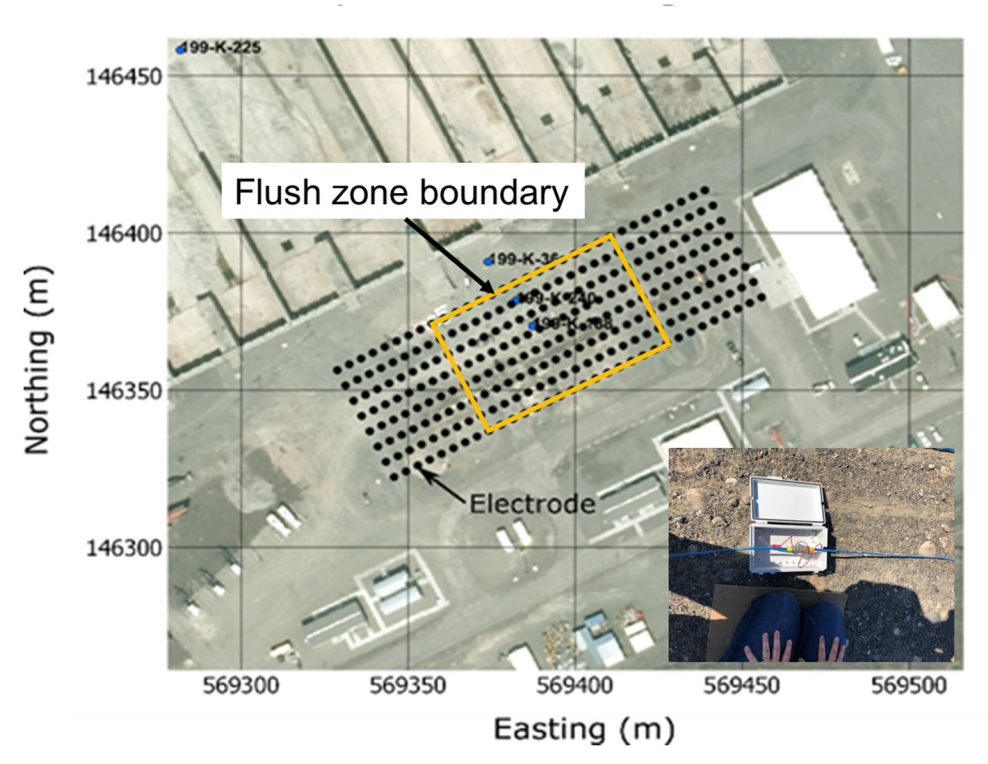


Figure 3. Location of surface ERT electrode lines (black dots) installed over the soil flushing zone. The lateral extent of the array, which impacts imaging depth of investigation, was limited by the building foundation located at the eastern margin of the array.

For perspective, Figure 4 (top) shows an oblique 3D view of the pit backfill boundary, flush zone boundary, electrode positions, extraction well positions, and the location of historical chromium handling infrastructure (i.e., tanks and piping systems) suspected of releasing chromium during site operations. Figure 4 (bottom) shows a vertical cross-section oriented perpendicular to the long axis of the infiltration zone, including the locations of the undisturbed Hanford and Ringold formations as interpreted from wellbore logs. The interface between the bottom of the pit backfill and the top of the Hanford formation is located at least 2 meters below the ground surface at its shallowest point within the soil flushing zone, and approximately 10 meters at its deepest. Consequently, all flush water applied at the surface migrates through a section of backfill material before reaching the Hanford formation interface. Furthermore, except for the pit bottom, the contact between backfill materials and the Hanford formation angles downward toward the bottom of the pit.

Ringold Fm. (sand and silt)

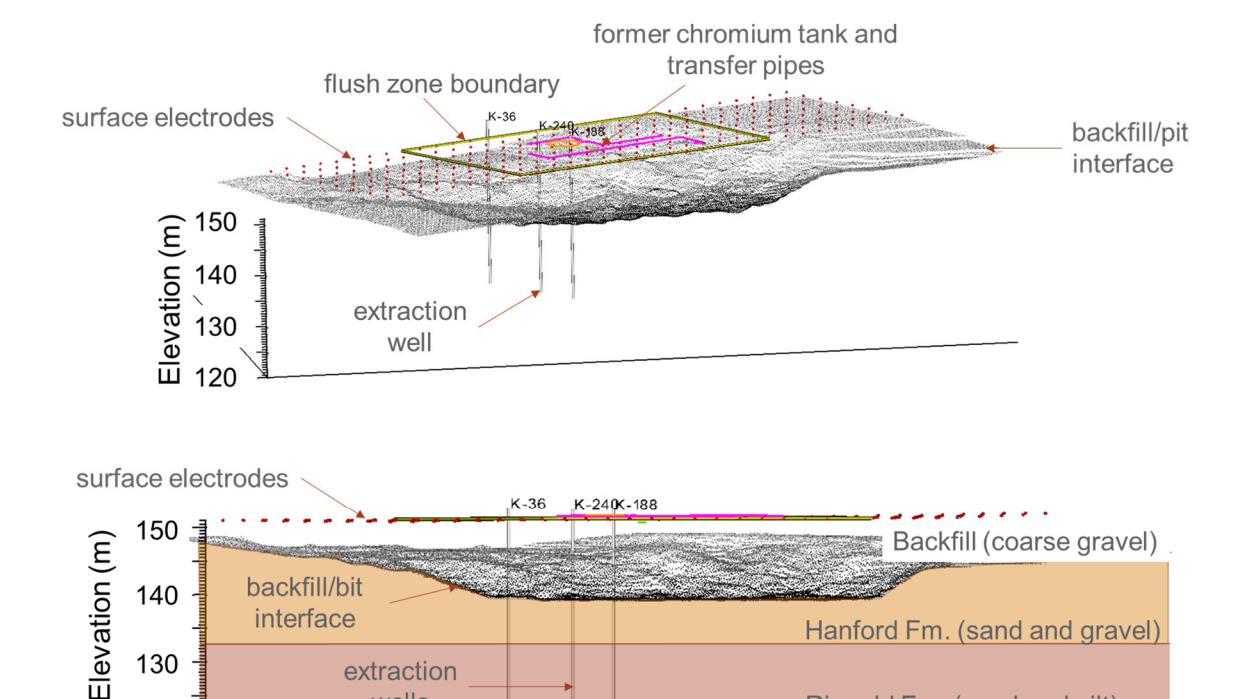


Figure 4. (top) Oblique view of the boundary between the pit backfill and the Hanford formation. (bottom) Cross section showing the approximate position of the water table, the Ringold Formation, the Hanford-Ringold formation contact, and the contact between the Hanford formation and pit backfill.

wells

120

Flush water was applied in three different zones (west, center, and east) within the infiltration gallery as shown in Figure 5A. Application rates in each zone over time are shown in Figure 5B. Flush water was applied continuously to the center zone with variable flow rate for the 49 days of flushing. In the east and west zones, flush water was applied intermittently for the first 21 days, and with continuously increasing flowrate after 21 days. The total application rate increased continuously to a maximum of ~431 lpm (114 gpm) after 49 days of flushing. This report is focused on ERT data collected during the first 28 days of flushing.

Figure 6 shows two photographs of the soil flushing system operating during the first week of flushing. Flush water application lines are shown in Figure 6 (left), and the ERT array (i.e., white boxes connected by cables) is shown in Figure 6 (right). Of note is the distribution of shallow surface ponding shown in Figure 6 (right), caused by slight variations in surface topography. Regions of ponding may facilitate the development of preferred vadose flow paths within the backfill soils.

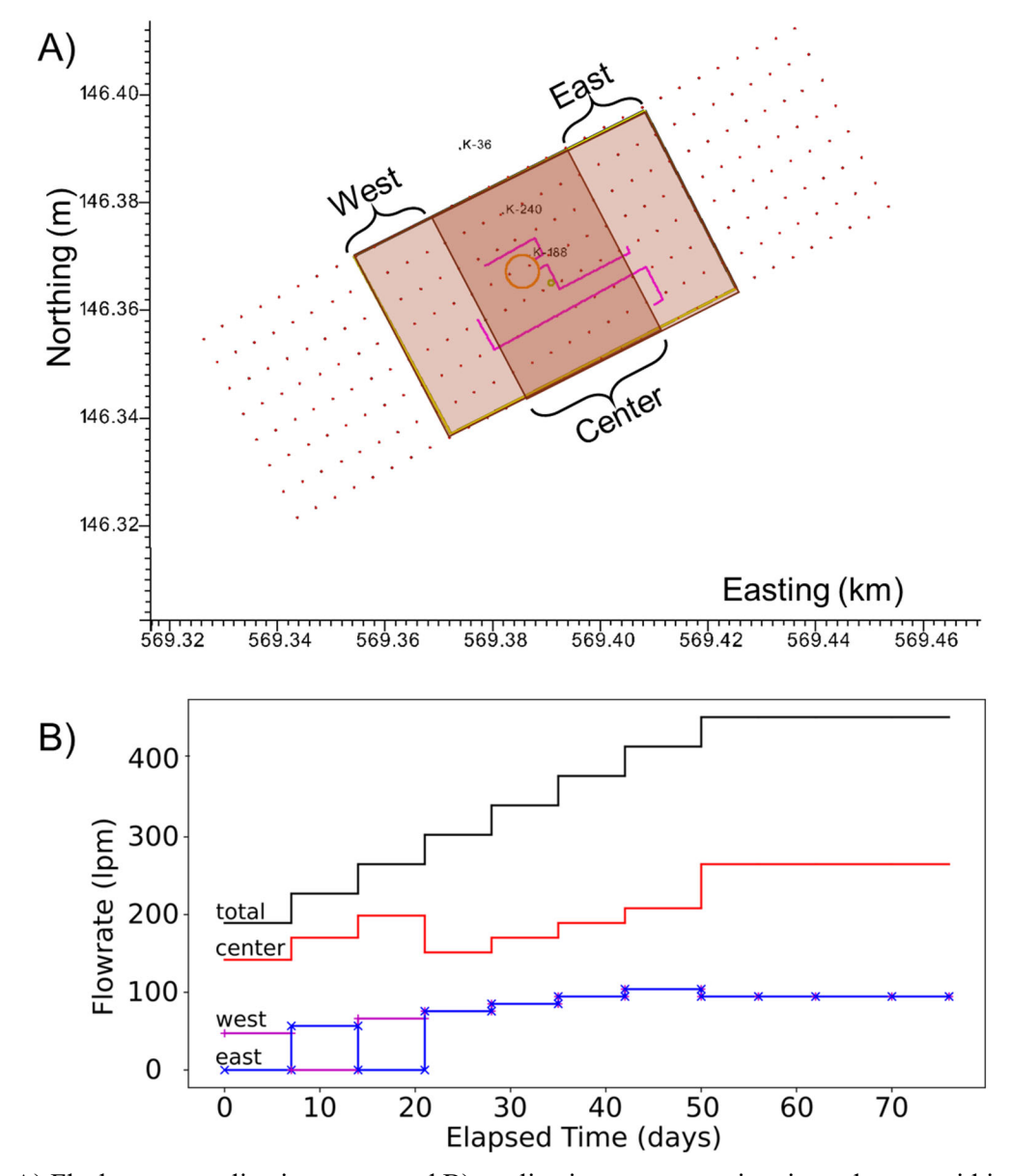


Figure 5. A) Flush water application zones and B) application rates over time in each zone within the infiltration gallery.

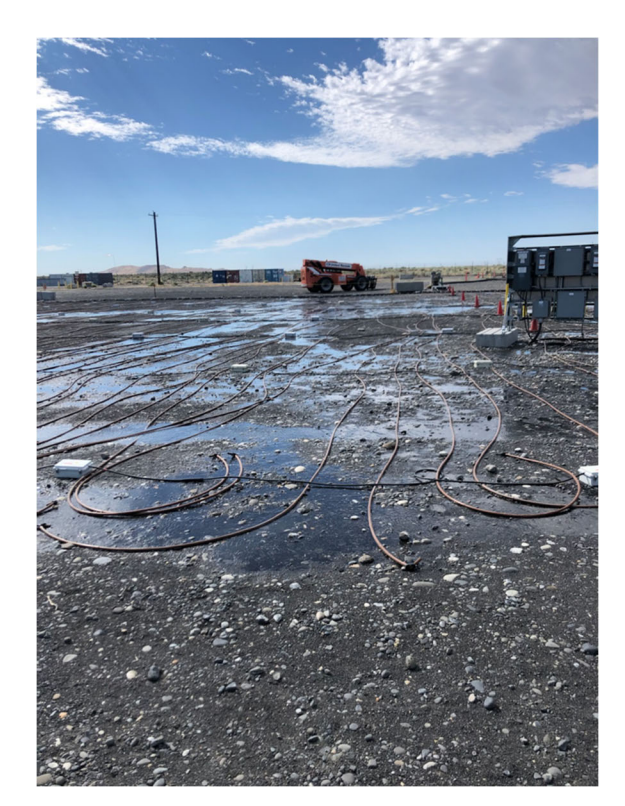




Figure 6. (left) Photograph taken during the first week of soil flushing, highlighting the distribution of flush water lines and shallow surface water ponding cause by slight variations in topography. (right) Photograph highlighting the ERT electrode array (white boxes connected by cables)

3.0 Time-Lapse ERT Imaging Summary and Interpretation

This section summarizes the Central Plateau Cleanup Company-supported time-lapse ERT monitoring results collected during the first 28 days of soil flushing in the 2023 campaign. ERT data was collected and autonomously processed using PNNL's E4D code (Johnson et al. 2010) every 2 hours for the full duration of the soil flushing operations. Figure 7 through Figure 10 provide summary images and corresponding interpretations of flush water flow paths for the first 28 days of flushing. Each figure shows the increase in BEC (warm colors) caused by the presence of flush water in three different cross-sections at 10-m offsets perpendicular to the ERT lines. The bottom cross-section (cross-section 1) traverses the deepest portion of the pit backfill, while the middle and upper cross-sections move north-westward and traverse progressively shallower portions of the pit. The contact between backfill materials and the Hanford formation is superimposed on each cross-section (white line) to aid interpretation of the ERT images, and magenta arrows designate the active flushing zones for the 7 days prior to the time when the image was collected. Figure 7 through Figure 10 show cross-sections for days 7, 14, 21, and 28, respectively, after the commencement of soil flushing. Depth resolution only extends 5 to 10 meters below the pit boundary, so the absence of changes in BEC at depth does not indicate the absence of flush water.

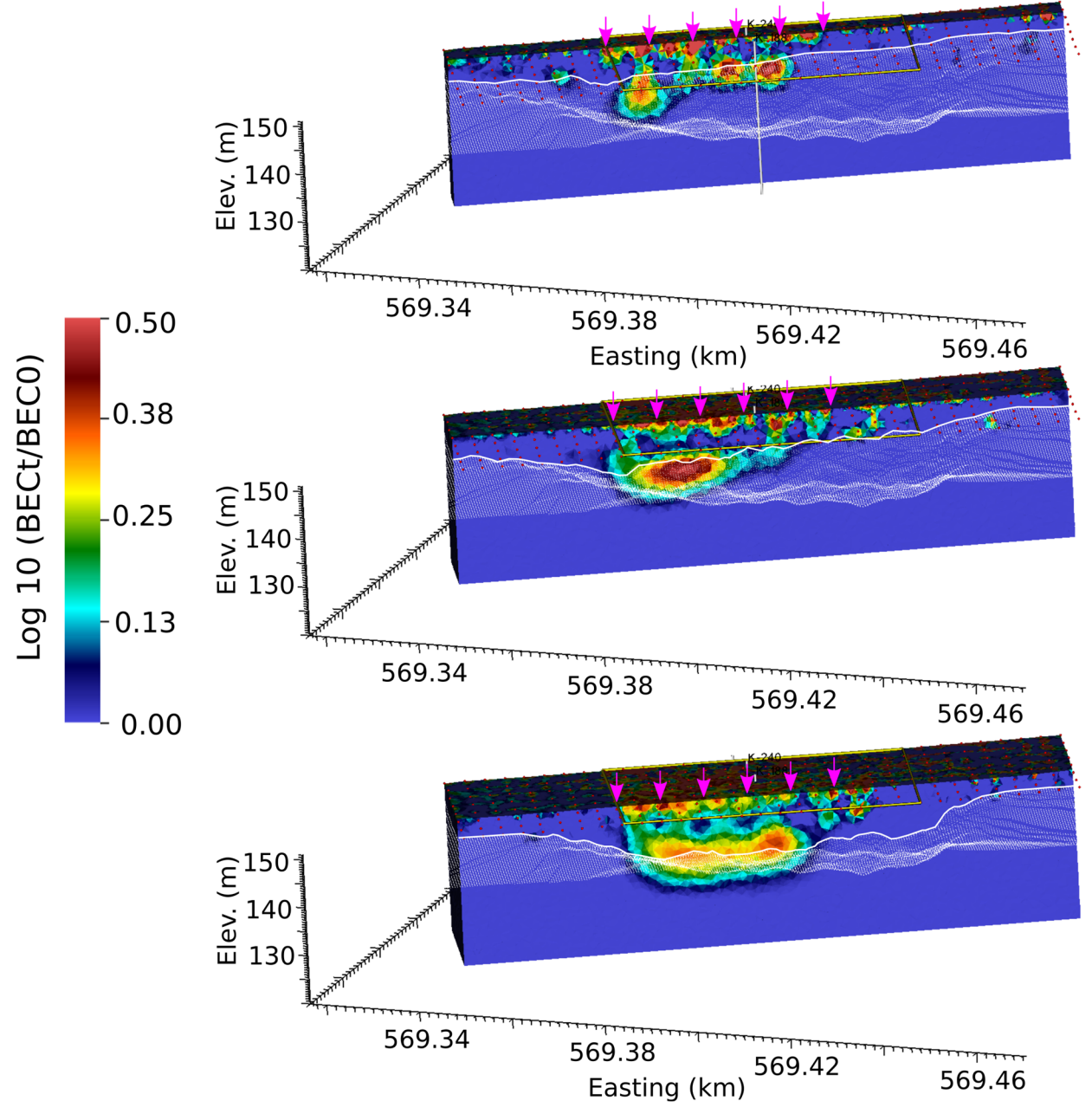


Figure 7. Summary of time-lapse ERT images after the first 7 days of flushing, highlighting the development of preferential flow paths within the pit backfill soils and redistribution of flush water along the pit boundary. Magenta arrows indicate the active flushing zone for the previous 7 days. White dappled surface is the pit boundary, and the white line denotes the pit boundary projected on the cross-section.

Figure 7 illustrates the development of preferential flow paths, or finger flow, within the backfill sediments, evident as horizontal discontinuities in BEC within the pit soils. Finger flow is a common phenomenon in vadose infiltration scenarios (Jarvis, Koestel, and Larsbo 2016, Kung 1990, Glass, Parlange, and Steenhuis 1989, Glass, Steenhuis, and Parlange 1989, Glass et al. 1990). Its occurrence becomes more likely as hydraulic conductivity and/or infiltration rate increases. In each cross-section shown in Figure 7, finger flow paths appear to enhance over time, which is consistent with both the increasing flush water application rates (Figure 5) and the increase in unsaturated hydraulic conductivity

known to occur as sediments become more saturated. Furthermore, the development of finger-flow in the backfill sediment may have been facilitated by the shallow surface ponding shown in Figure 6, where preferential flow paths develop beneath the ponding zones.

Figure 7 through Figure 10 also highlight the influence of the interface between the backfill and Hanford formation sediments on flush water flow paths. In the upper cross-sections, which intersect sloped portions of the pit boundary, it is evident that flush water supplied from preferential flow paths within the backfill redistributes along the pit boundary surface. Furthermore, minimal infiltration below the pit boundary suggests flush water migrates down-slope along the boundary surface, as opposed to downward vertically through the boundary. In the center cross-section of each figure, it is apparent that the flush water congregates at a low point in the pit boundary before moving vertically downward beneath the western end of the infiltration gallery. The high BEC zone appears to be disconnected from the surface for most of the center cross-sections images, suggesting the flush water congregating at the low point in the pit boundary is supplied from out-of-plane (e.g., from the northward region of the pit boundary). In each of the bottom cross-sections, it is clear that the flush water moving through preferential flow paths in pit soils is redistributed laterally along the deepest part of the pit and moves vertically downward into the Hanford formation without any apparent finger flow. Redirection of flow along the pit boundary appears to direct flush water to the bottom of the pit boundary, and likely has a significant influence on which regions of the Hanford and Ringold formations received flush water. These results also suggest the backfill materials are more permeable than the Hanford formation.

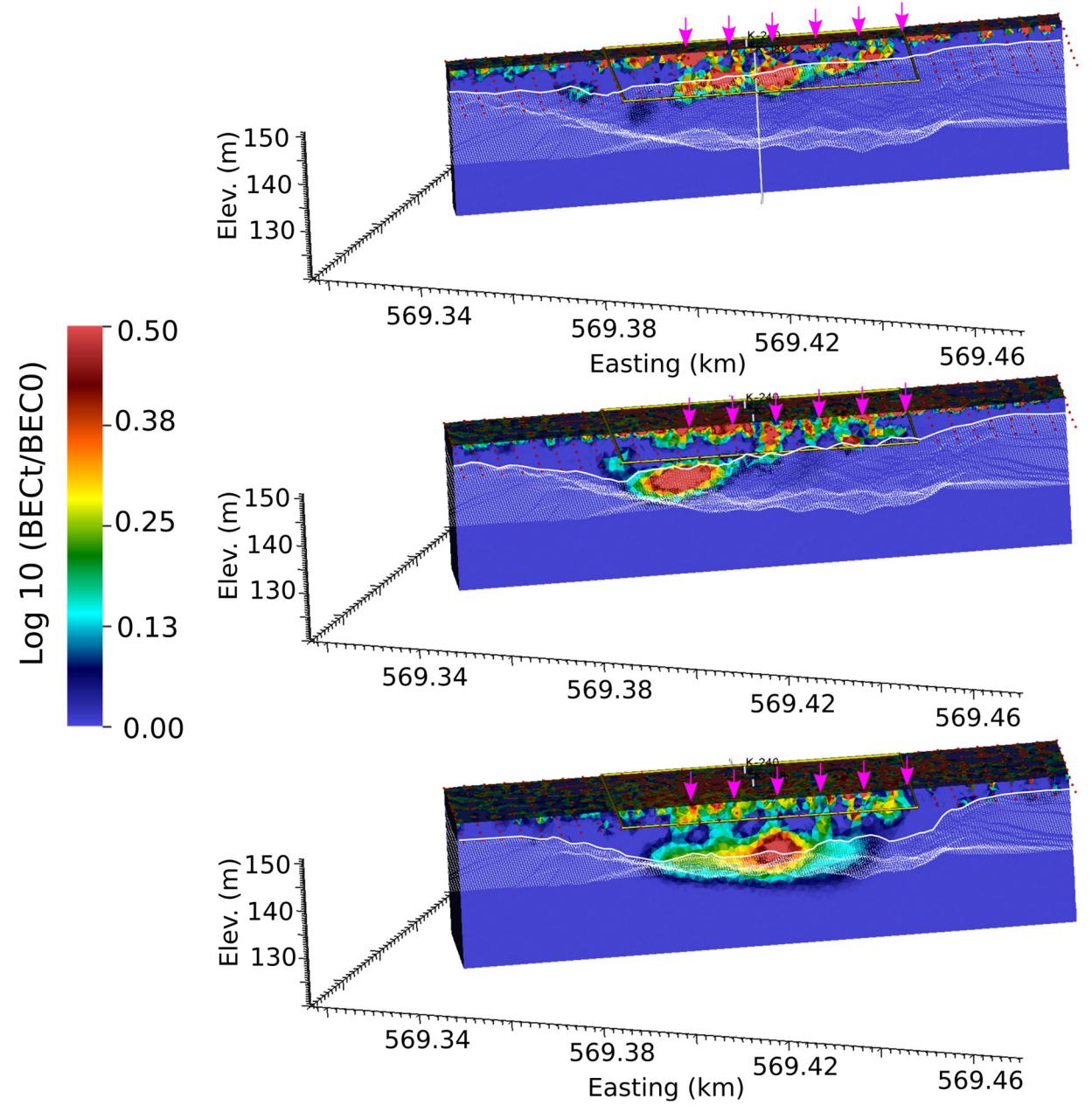


Figure 8. Summary of time-lapse ERT images after the first 14 days of flushing, highlighting the development of preferential flow paths within the pit backfill soils and redistribution of flush water along the pit boundary. Magenta arrows indicate the active flushing zone for the previous 7 days. White dappled surface is the pit boundary, and the white line denotes the pit boundary projected on the cross-section.

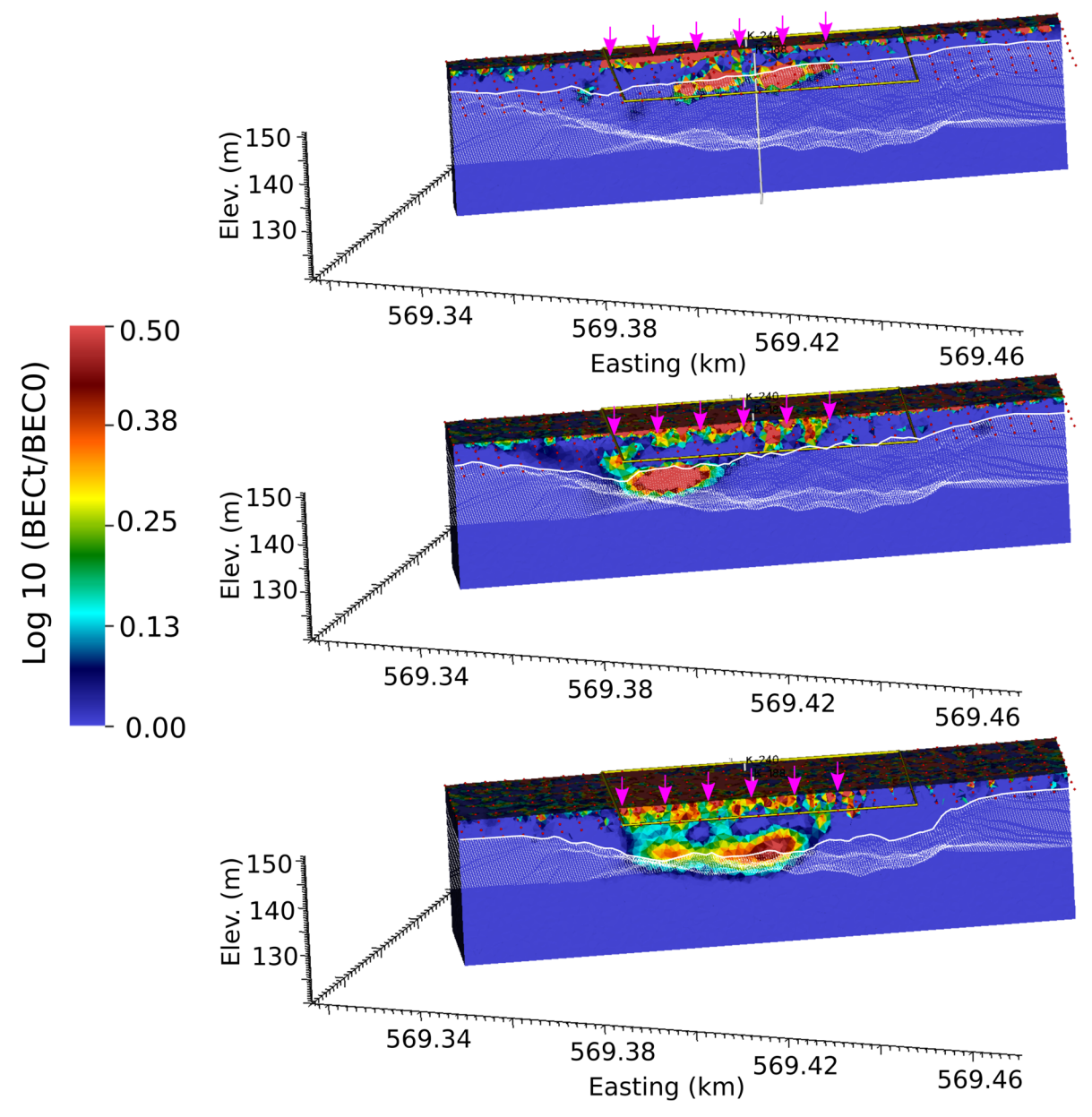


Figure 9. Summary of time-lapse ERT images after the first 21 days of flushing, highlighting the development of preferential flow paths within the pit backfill soils and redistribution of flush water along the pit boundary. Magenta arrows indicate the active flushing zone for the previous 7 days. White dappled surface is the pit boundary, and the white line denotes the pit boundary projected on the cross-section.

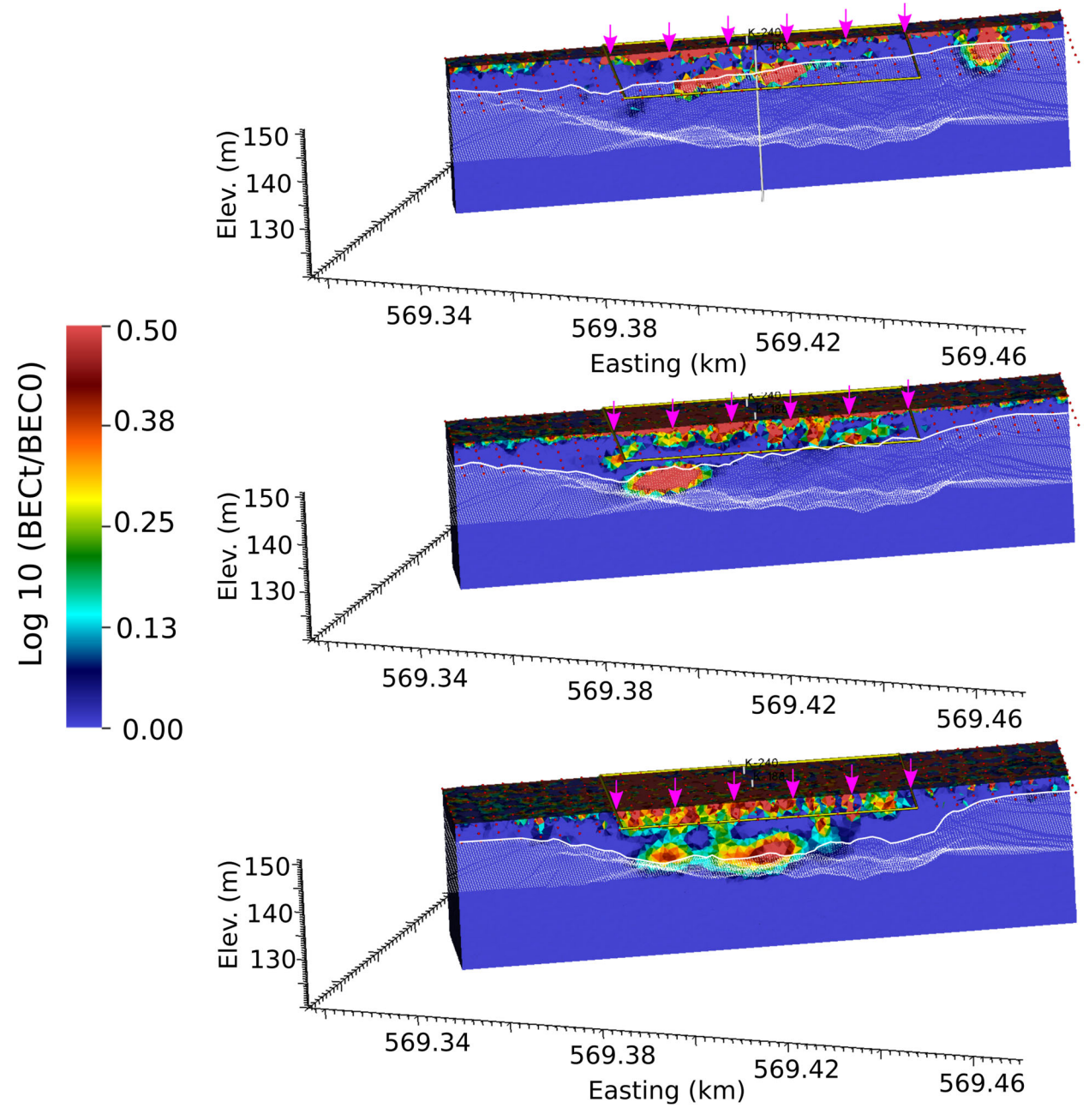


Figure 10. Summary of time-lapse ERT images after the first 28 days of flushing, highlighting the development of preferential flow paths within the pit backfill soils and redistribution of flush water along the pit boundary. Magenta arrows indicate the active flushing zone for the previous 7 days. White dappled surface is the pit boundary, and the white line denotes the pit boundary projected on the cross-section.

4.0 ERT-Based Deep Neural Network Training and Prediction of Field Soil Flushing Behavior

This section describes progress toward building a digital twin of the 100 KE soil flushing system, which is a numerical simulation that honors available monitoring data collected during flushing operations, including ERT monitoring data. The conceptual model includes the three distinct stratigraphic units shown in Figure 4, including pit backfill, Hanford formation, and Ringold formation soils, and their corresponding unsaturated hydraulic properties and petrophysical relationships. Petrophysical relationships for each unit describe the relationship between BEC and porosity, saturation, pore fluid conductivity, and surface conductivity, represented in the form of Archie's law (Archie 1942).

Generating the digital twin involves estimating the hydrogeologic properties and petrophysical relationships for each stratigraphic unit, and the fluid conductivity of the native pore water and the flush water. Hydrogeologic parameters that must be estimated include porosity, horizontal permeability, vertical permeability, residual saturation, and the van Genuchten function Alpha and M fitting parameters (using the Mualem saturation function). Petrophysical parameters that must be estimated include Archie's law cementation exponent, saturation exponent, tortuosity constant, and surface conductivity. In total, nine parameters per stratigraphic unit plus the native pore water conductivity and the flush water conductivity are estimated to generate the digital twin (29 parameters total).

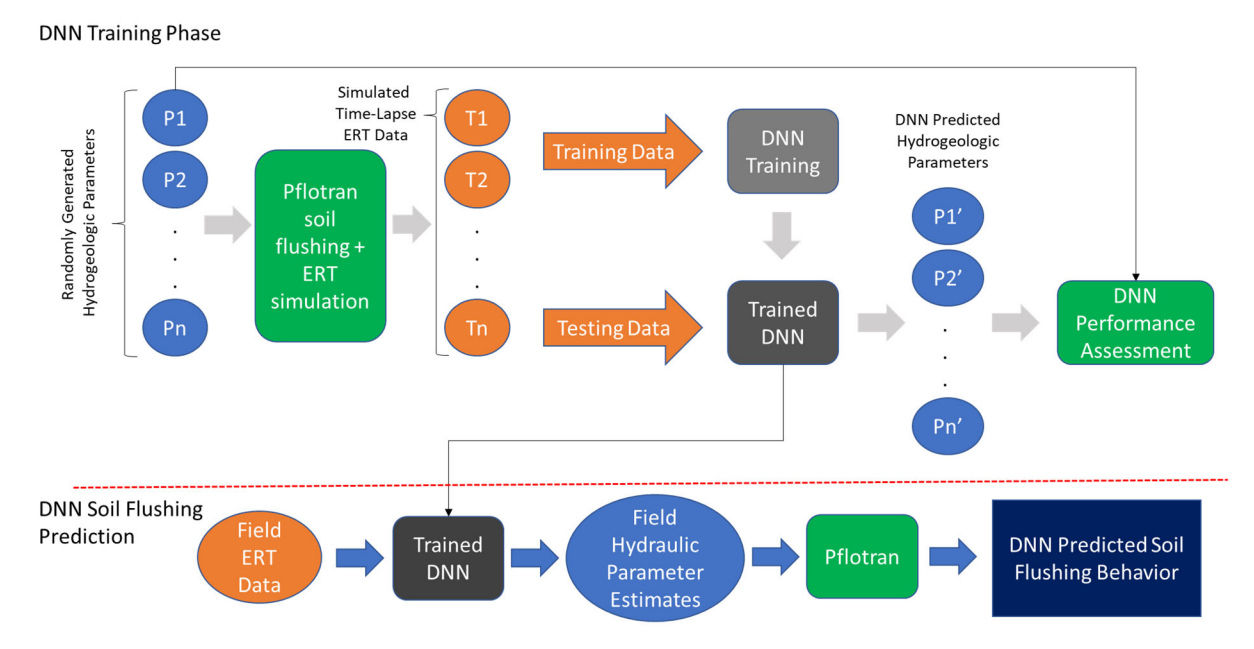


Figure 11. Flow diagram showing training and application of a deep neural network for prediction of soil flushing behavior using field ERT monitoring data.

Model parameters will ultimately be estimated using new joint hydro-geophysical inversion capabilities recently implemented in the massively parallel PFLOTRAN subsurface simulation code (Jaysaval et al. 2023). However, a well-known limitation of joint inversion involves the occurrence of local minima, which causes the inversion to converge to a non-optimal solution if the initial guess is far from the optimum. To provide an accurate starting model and reduce the risk of converging to local minima, PFLOTRAN was used to train a deep neural network (DNN) to estimate each of the 29 model parameters using the time-lapse ERT data collected during the first 28 days of soil flushing. A flow chart for the DNN training and parameter estimation is shown in Figure 11. In the training phase, model realizations

are generated by selecting each of the 29 parameters from uniform random distributions with physically realistic bounds for each stratigraphic unit. Bounds on porosity and van Genuchten parameters were chosen as the maximum and minimum values reported in Table 1 of Khaleel and Freeman (1995), who measured Hanford 200 Area soils classified as SS (sand mixed with finer fraction), S (sand), SSG (sand and gravel mixed with finder fraction), GS (gravelly sand), SG1 (sandy gravel with gravel fraction < 60%), and SG2 (sandy gravel with gravel fraction > 60%). Horizontal intrinsic permeability bounds were chosen as 1e-13 m² to 1e-7 m² for all soils. The ratio of vertical to horizontal intrinsic permeability was bounded between 0.2 and 1.0 for all soils. Archie's cementation exponent (commonly assumed to be 1.3 for unconsolidated sediments) was bounded between 1.1 and 2.1; Archie's saturation exponent (commonly assumed to be 2.0 for unconsolidated soils) was bounded between 1.6 and 2.6; Archie's tortuosity factor (commonly assumed to be 1.0 for unconsolidated sediments), was bound between 0.8 and 1.2; and soil surface conductivity was bound between 1e-5 and 1e-2 S/m for all soils.

Each random parameter set is used as input to PFLOTRAN, which simulates the ERT data time series collected during soil flushing for each simulation. Next, random noise is added to the ERT data and the realizations are randomly divided, with 75% of the realizations used for DNN training, and 25% used to assess the performance of the DNN. Once the DNN is trained with the training data set, the test realizations are input to the DNN, which then predicts the 29 model parameters corresponding to each realization. Finally, the predicted model parameters are statistically compared to the true model parameters to assess DNN performance.

Assuming the conceptual model used to generate the training data is sufficiently accurate (i.e., homogenous properties in each stratigraphic unit, uniform flush water application, etc.), the DNN performance assessment provides quantitative metrics regarding the capability of the ERT data to resolve the 29 estimated parameters. For example, if the trained DNN can predict parameters with a high degree of fidelity using the test data sets, then the training data must collectively contain enough independent information about the parameters to independently resolve each one. Comparisons between true and DNN-predicted parameters provide a natural assessment of uncertainty in the estimated parameters, which can be extended to uncertainty in soil flushing behavior through simulation. Conversely, if the DNN cannot be trained to accurately predict the test parameters (within 10% of the true values), then there may not be sufficient information in the training data to resolve the parameters. In either case, uncertainty in parameter predictions is a natural outcome of the DNN performance assessment.

Initial testing of the DNN prediction capabilities used 200 generated realizations, 150 for training and 50 for performance assessment. Standard deviations of the prediction error for each parameter were under 5% for each of the parameters in the backfill soil and Hanford formation. Prediction errors were larger for Ringold Formation sediments, presumably because the ERT data has limited sensitivity at the depth of the Ringold Formation.

To generate the starting model for the joint inversion, the field ERT data are applied to the trained DNN as shown in the lower flowchart in Figure 11, resulting in 29 parameters that, given an accurate conceptual model, should honor the true 100 KE soil parameters within the 5% error range suggested by the DNN performance assessment. However, the conceptual model does not consider some aspects of the system that are present in reality, the foremost being heterogeneity within each of the stratigraphic units, unequal distribution of the flush water at the surface, and preferential flow paths within the backfill soil. The effects of variations in flush water temperature and/or fluid conductivity, or geochemical reactions that may alter fluid conductivity, are also not considered, although they are expected to be small. For these reasons, the DNN-based parameter estimates generated using field data are expected to be less accurate than estimates generated using synthetic data to a degree that hasn't yet been quantified. Regardless, the DNN is trained to provide generalized parameter estimates based on data trends, and is

anticipated to provide a starting model that is closer to a global minimum (i.e., closer to the true field parameters) than is otherwise available.

Table 1 shows the parameter estimates for each stratigraphic unit predicted by the DNN using ERT monitoring data collected during the first 28 days of operation. Some characteristics of the predictions are consistent with the ERT images and interpretations presented in Section 3.0. First, the permeability of the backfill is greater than the permeability of the Hanford formation – a condition necessary to enable flush water redirection along the boundary between the backfill soils and the Hanford formation. Horizontal permeability is predicted to be greater the vertical permeability in each stratigraphic unit, which is a predominant condition encountered in sedimentary depositional systems. Flush water electrical conductivity is predicted to be 0.064 S/m, which is about six times the predicted native pore water conductivity, but within the range of observed field values of flush water conductivity (0.044 to 0.067 S/m¹).

	Pit Backfill	Hanford Formation	Ringold Formation
	I It Dackiiii	Haillolu Polillation	Kiligola Formation
Porosity	2.34E-01	2.58E-01	3.23E-01
Horizontal Permeability (m^2)	1.85E-11	1.22E-12	2.07E-13
Vertical Permeability (m^2)	1.11E-11	8.10E-13	1.50E-13
Residual Saturation	1.00E-03	8.00E-02	1.00E-03
van Genuchten Alpha (1/Pa)	8.03E-04	7.10E-02	8.03E-04
van Genuchten M	3.40E-01	3.19E-01	3.40E-01
Archie Cementation Exp.	1.22E+00	1.88E+00	1.28E+00
Archie Saturation Exp.	1.68E+00	2.26E+00	2.32E+00
Archie Tortuosity Constant	9.80E-01	1.11E+00	1.08E+00
Archie Surface Cond. (S/m)	2.00E-04	9.10E-05	1.10E+00
Native Pore Water Cond. (S/m)		1.55E-02	_
Flush Water Cond. (S/m)		6.36E-02	

Table 1. DNN-predicted 100 KE soil hydraulic properties and petrophysical parameters.

In addition to being used as the starting model for the joint inversion (which is in progress), the DNN-based parameter estimate can be used to simulate general soil flushing behavior. Although the simulation will not account for the effects of intra-unit heterogeneity, surface ponding, or temperature variations among other factors, it will provide behavior predictions that honor the ERT data, obey physical laws of unsaturated zone transport, and may accurately predict the general behavior of flush water in the subsurface. For example, Figure 12 through Figure 15 respectively show the simulated progression of the increase in soil saturation along three cross-sections after 7, 14, 21, and 28 days of flushing. Each figure also includes cross-sections showing interfaces between stratigraphic units to aid in demonstrating the impact of interface between the backfill and Hanford formation, and of the Hanford/Ringold contact. These images are essentially DNN predictions of 100 KE soil flushing behavior given the ERT monitoring data.

Figure 12 shows the predicted increases in saturation after the first 7 days of flushing in the west and central flushing zones. Immediately evident is the increase in saturation that occurs across the backfill/Hanford formation interface in the shallow (top two) cross-sections. This effect is caused by the decrease in permeability from the backfill to the Hanford formation and the corresponding requirement to

¹Jeremy Lynn (CPCCo), 03/09/2023.

maintain mass balance of flush water. In the bottom cross-section where the backfill is deeper, flush water is just beginning to arrive at the Hanford formation on day 7. Although the DNN predicted flush behavior does not capture the preferential flow paths through the backfill material that are evident in the ERT images, the increase in saturation (and therefore BEC) at the backfill/Hanford formation interface is consistent between the two in terms of general flow behavior.

With the exception of the preferential flow path in the backfill soil, and with the understanding that the ERT images do not resolve flush water behavior at the deeper Hanford/Ringold contact, the DNN predictions are generally consistent with the ERT images through day 28; however, the DNN predictions reveal notable behaviors that are not resolvable by the ERT imaging.

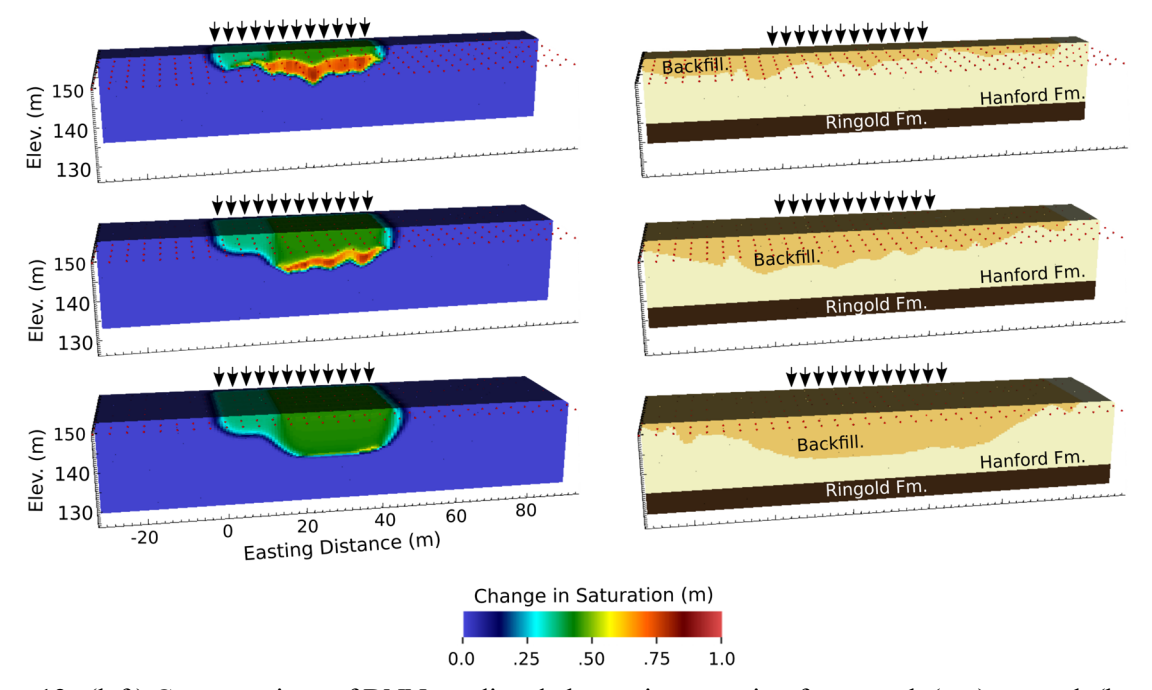


Figure 12. (left) Cross-sections of DNN-predicted change in saturation from north (top) to south (bottom) after 7 days of flushing in west and center flushing zones. (right) Stratigraphic cross-section.

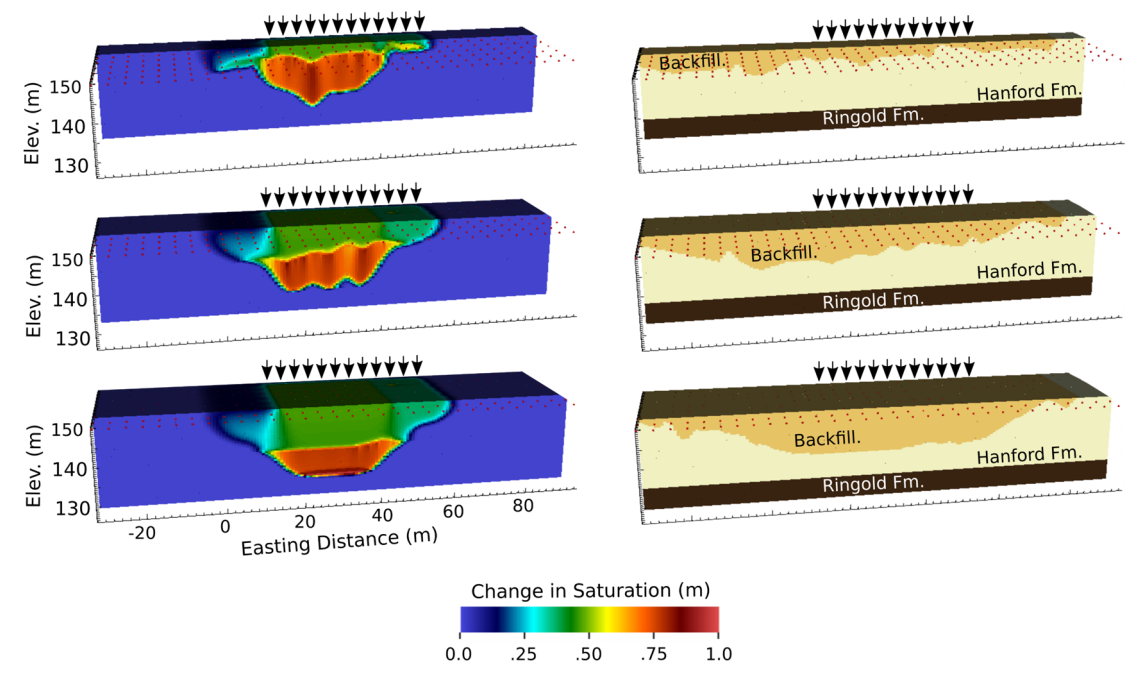


Figure 13. (left) Cross-sections of DNN-predicted change in saturation from north (top) to south (bottom) after 14 days of flushing. Center and east flushing zones were active from day 7 to day 14 (see Figure 5). (right) Stratigraphic cross-sections corresponding to each saturation cross-section.

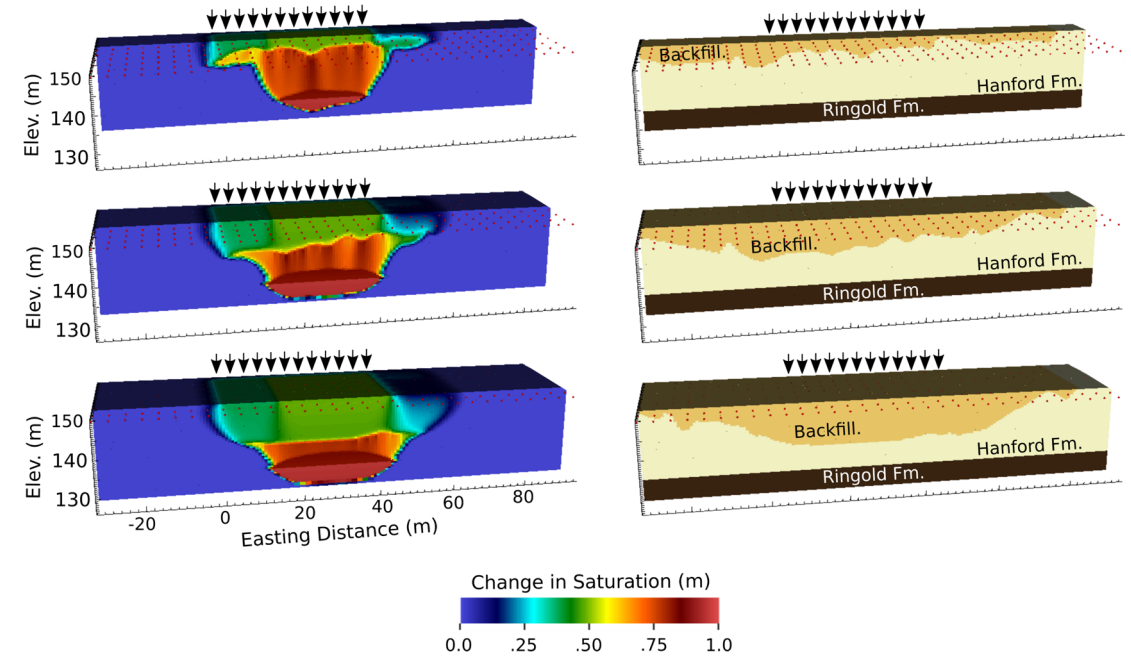


Figure 14. (left) Cross-sections of DNN-predicted change in saturation from north (top) to south (bottom) after 21 days of flushing. Center and west flushing zones were active from day 14 to day 21 (see Figure 5). (right) Stratigraphic cross-sections corresponding to each saturation cross-section.

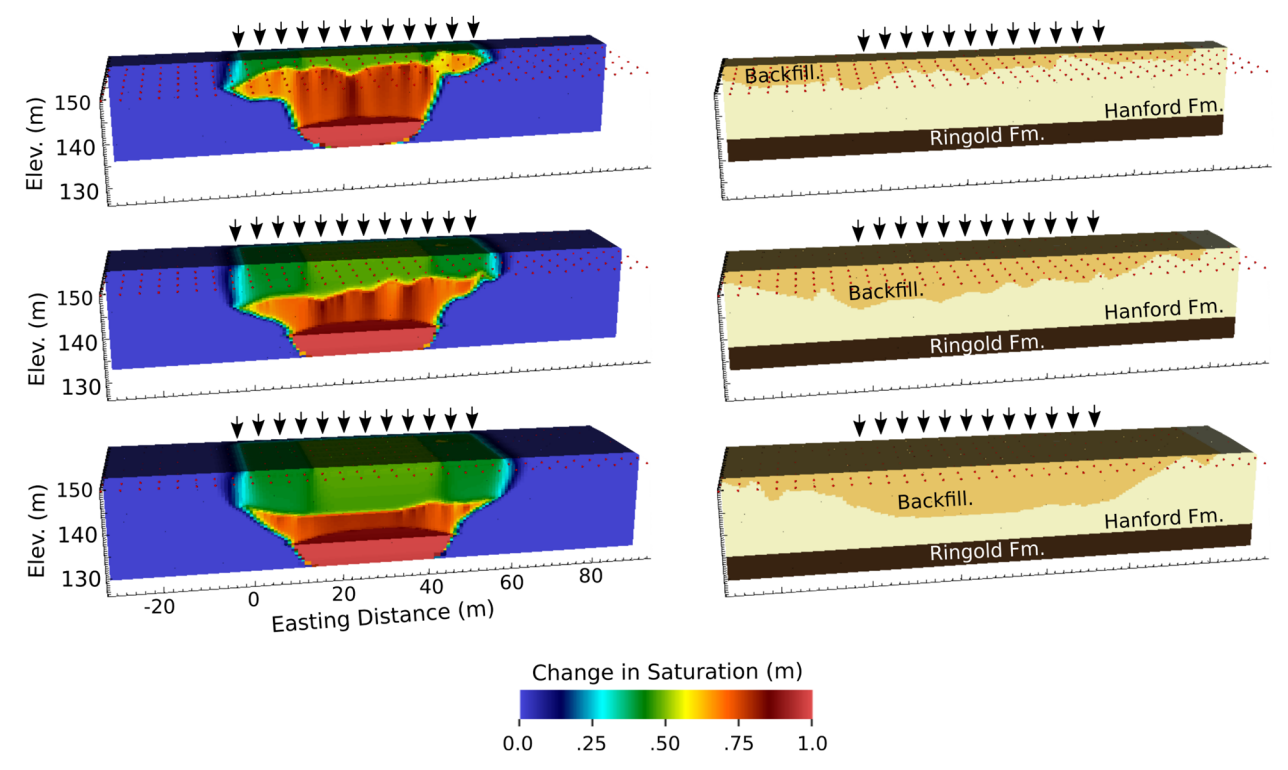


Figure 15. (left) Cross-sections of DNN-predicted change in saturation from north (top) to south (bottom) after 28 days of flushing. All flushing zones were active from day 21 to day 28 (see Figure 5). (right) Stratigraphic cross-sections corresponding to each saturation cross-section.

For example, within the Hanford formation, saturation levels are higher beneath tomographic lows in the pit boundary, again suggesting that flush water is redirected to low points in the boundary. In addition, the footprint of the flush water treatment decreases significantly with depth in comparison to the application footprint at the surface, largely due to the redirection of flush water to the bottom of the pit boundary.

5.0 Discussion and Next Steps

This project represents a first-of-its-kind effort to directly inform a predictive simulator with time-lapse geophysical monitoring data, with the ultimate objective of using that simulator to accurately assess the behavior of subsurface processes (soil flushing in this case). The capability to develop a representative digital twin of the subsurface has long been hindered by a lack of sufficient information to adequately estimate system-governing parameters. In this case, we are using time-lapse ERT monitoring data to address the information gap. Consequently, success or failure in generating an accurate predictive simulation of 100 KE soil flushing behavior hinges directly on the value of information in the ERT data time-series, specifically regarding the unsaturated hydraulic properties that govern flush water transport. We have thus far used multi-physics simulations and deep machine learning to demonstrate at a minimum that if (1) soil hydraulic properties can be considered homogenous within each of the three primary stratigraphic units in the system and (2) uniform application of flush water at the surface is a valid approximation, then there is sufficient information in the time-lapse ERT data to accurately estimate governing hydraulic properties of the backfill and Hanford formation, and to a lesser extent the Ringold Formation.

The advantages of assessing soil flushing behavior using simulation over ERT imaging alone are numerous, and include (but are not limited to) the following:

- The digital twin assessment is bound by the physics of flow and transport, while the ERT images are not (i.e., they are smeared due to limited resolution).
- The analysis provides valuable in situ estimates of soil hydraulic properties.
- The digital twin can be used to extract qualitative performance metrics, such as the number of pore volumes of flush water moving through a given region of the subsurface.
- The digital twin can be used to design and predict the performance of future remediation actions at the same site.

The primary limitation is that errors in the conceptual model may lead to poor predictions of soil hydraulic properties and soil flushing behavior. Consequently, uncertainty estimation is a required for comprehensive analysis of the predictive simulations.

Next steps in the development and demonstration include:

- Refining and publishing the DNN assessment of the information value in time-lapse ERT data
- Joint inversion using the DNN-based estimate as the starting model
- Source-term inversion, whereby the digital twin and chromium concentration time series from the 100 KE extraction well are used within a secondary inversion to identify the possible range of locations and concentrations of soil sources

We will submit a second peer-reviewed publication on this topic as a deliverable for fiscal year 2024.

6.0 Quality Assurance

This work was performed in accordance with the Pacific Northwest National Laboratory (PNNL) Nuclear Quality Assurance Program (NQAP). The NQAP complies with the United States Department of Energy Order 414.1D, Quality Assurance. The NQAP uses NQA 1 2012, Quality Assurance Requirements for Nuclear Facility Application as its consensus standard and NQA 1 2012 Subpart 4.2.1 as the basis for its graded approach to quality. This work emphasized acquiring new theoretical or experimental knowledge. The information associated with this report should not be used as design input or operating parameters without additional qualification.

Quality Assurance 22

7.0 References

- Archie, G. E. 1942. "The electrical resistivity log as an aid in determining some reservoir characteristics." Transactions of the American Institute of Mining and Metallurgical Engineers 146:54-61. doi: 10.2118/942054-G.
- Glass, R. J., S. Cann, J. King, N. Baily, J. Y. Parlange, and T. S. Steenhuis. 1990. "Wetting Front Instability in Unsaturated Porous-Media a 3-Dimensional Study in Initially Dry Sand." Transport in Porous Media 5 (3):247-268. doi: Doi 10.1007/Bf00140015.
- Glass, R. J., J. Y. Parlange, and T. S. Steenhuis. 1989. "Wetting Front Instability .1. Theoretical Discussion and Dimensional Analysis." Water Resources Research 25 (6):1187-1194. doi: 10.1029/WR025i006p01187.
- Glass, R. J., T. S. Steenhuis, and J. Y. Parlange. 1989. "Wetting Front Instability .2. Experimental-Determination of Relationships between System Parameters and Two-Dimensional Unstable Flow Field Behavior in Initially Dry Porous-Media." Water Resources Research 25 (6):1195-1207. doi: 10.1029/WR025i006p01195.
- Jarvis, N., J. Koestel, and M. Larsbo. 2016. "Understanding Preferential Flow in the Vadose Zone: Recent Advances and Future Prospects." Vadose Zone Journal 15 (12). doi: 10.2136/vzj2016.09.0075.
- Jaysaval, P., G. E. Hammond, and T. C. Johnson. 2023. "Massively parallel modeling and inversion of electrical resistivity tomography data using PFLOTRAN." Geoscientific Model Development 16 (3):961-976. doi: 10.5194/gmd-16-961-2023.
- Johnson, T. C., R. J. Versteeg, A. Ward, F. D. Day-Lewis, and A. Revil. 2010. "Improved hydrogeophysical characterization and monitoring through parallel modeling and inversion of time-domain resistivity and induced-polarization data." Geophysics 75 (4):Wa27-Wa41. doi: 10.1190/1.3475513.
- Khaleel, R., and E. J. Freeman. 1995. "Variability and Scaling of Hydraulic Properties for 200 Area Soils, Hanford Site." US DOE. https://www.osti.gov/servlets/purl/188564
- Kung, K. J. S. 1990. "Preferential Flow in a Sandy Vadose Zone .2. Mechanism and Implications." Geoderma 46 (1-3):59-71. doi: 10.1016/0016-7061(90)90007-V.

References 23

Pacific Northwest National Laboratory

902 Battelle Boulevard P.O. Box 999 Richland, WA 99354

1-888-375-PNNL (7665)

www.pnnl.gov